A new look to Multichannel Blind Image Deconvolution

W. Souidene[1,4], K. Abed-Meraim[2,3], A. Beghdadi[4]
[1] ESIGETEL, 1 rue du port de Valvins, 77215 Avon-Fontainebleau
[2] Telecom ParisTech, 46 rue Barrault, 75013, Paris
[3] University of Sharjah, College of Engineering, ECE Dept. UAE
[4] L2TI, Université Paris 13, 99 av. J.B Clément 93430, Villetaneuse
wided.souidene@esigetel.fr, kmeriam@sharjah.ac.ae, beghdadi@l2ti.univ-paris13.fr

***Abstract*—The aim of this paper is to propose a new look to MBID, examine some known approaches and provide a new MC method for restoring blurred and noisy images. First the direct image restoration problem is briefly revisited. Then a new method based on inverse filtering for perfect image restoration in the noiseless case is proposed. The noisy case is addressed by introducing a regularization term into the objective function in order to avoid noise amplification. Second, the filter identification problem is considered in the MC context. A new robust solution to estimate the degradation matrix filter is then derived and used in conjunction with a total variation approach to restore the original image. Simulation results and performance evaluations using recent image quality metrics are provided to assess the effectiveness of the proposed methods.**

I. Introduction

Multichannel (MC) image processing is nowadays a relatively active field of research. Preliminary results of multichannel deconvolution were first found in the signal case then extended to the image. This development is due to the increasing number of applications where several versions of the captured image are available. In multichannel framework, several images are observed from a single scene that passes through different channels. Applications where multichannel techniques could be used include, among others, polarimetric [1], satellite [2], astronomical [3], [4] and microscopic [5] imagery. When channels are frequency bands, we refer to it as multi-spectral images. If the same scene is captured at different time slots, we talk about image sequences. If different representations of the same image are provided at different resolutions, we also can treat this as a multichannel representation. The main advantage we can draw from MC processing for the deconvolution is to exploit the diversity and redundancy of information in the different acquisitions. Hence, it is worth to note that the set of the observed images is considered as one entity.

Image deconvolution/restoration solutions can be divided into two classes : stochastic and deterministic. Stochastic methods consider observed images as random fields and estimate the original image as the most probable realization of a certain random process. These methods are, mainly, the Linear Minimum Mean Squares Error (LMMSE) [6], the Maximum Likelihood (ML) [7] and the Maximum A Posteriori (MAP) [8]. These methods have two major drawbacks: (i) they are very sensitive to perturbations and modeling errors, (ii) strong statistical hypothesis are made on the image and the noise which are considered as uncorrelated homogeneous random processes. On the other hand, deterministic methods do not rely on such hypothesis and estimate the original image by minimizing a norm of a certain residuum. These methods include among others: Constrained Least Square (CLS) methods which incorporate a regularization term [9], the iterative blind deconvolution technique [10] and the Non-negativity And Support constraint – Recursive Inverse Filtering (NAS-RIF) algorithm [11]. The latter methods are based on minimizing a certain criterion under some constraints like non-negativity of the original image, finite support of the convolution masks, smoothness of the estimate, etc...

Blind MC image deconvolution can be performed in two ways. One can first identify the point spread function (PSF) of the degradation also called blur function and then restore the image using this knowledge. This approach belongs to the class of identification techniques [12]. When the original image is directly restored, we refer to the solution as an equalization or inverse filtering technique. In this article, we deal with an equalization technique called the Mutually Referenced Equalizers (MRE) where a regularization term is incorporated is order to prevent from noise amplification. Then, we consider another approach which belongs to the class of channel identification techniques. We carry out a comparative study in order to choose the most efficient blind channel identification algorithm. We compared these techniques in terms of estimation accuracy (restored image quality), and identification accuracy (distance between the real and the identified filters). Finally, we develop a joint identification/restoration technique using the Total Variation (TV) aiming at the restoration of the original image.

More precisely, our contributions consist in (i) a new blind restoration method using the mutually referenced equalizers technique in conjunction with a regularization method that truncates the greatest singular values of the inverse filter matrix; (ii) a new multichannel identification technique that generalizes the Least Squares Smoothing (LSS) method [13] from the 1D to the 2D case. This method is then compared with other existing identification methods with respect to the estimation accuracy and computational cost; (iii) a new robust multichannel restoration method based on a total variation

technique and (iv) a performance evaluation and comparative study of the different blind restoration methods using some objective image quality metrics.
The rest of the paper is organized as follows. Section II highlights the advantages of the multichannel processing approach. Section III introduces the image acquisition model and states the objectives of this work. In section IV, the regularized MRE method is developed. Section V presents the generalized LSS method and briefly reviews some other existing channel identification algorithms for comparison purposes. In section VI, we introduce our image restoration technique using the total variation approach. Simulation results and performance evaluation are provided in section VII. The last section is for the conclusion and final remarks.

II. Motivations for MC processing

The motivations behind the use of MC framework as compared to the standard mono-channel one are first the increasing number of applications in this field, but more importantly, the potential diversity gain that may lead to significant improvements in the restored image quality. Indeed, diversity combining techniques have been recently the focus of an intensive research effort in different application fields including radar processing [14], wireless communications [15] and image processing [16]. It is shown in particular that, in the noiseless case, the diversity combining techniques allow a perfect image restoration [17]. This is illustrated by the example in figure 1 where we compare a blind mono-channel restoration technique developed in [18], and based on the iterative Richardson-Lucy scheme, with the multichannel one developed in section IV of this article. Clearly, this example highlights the performance

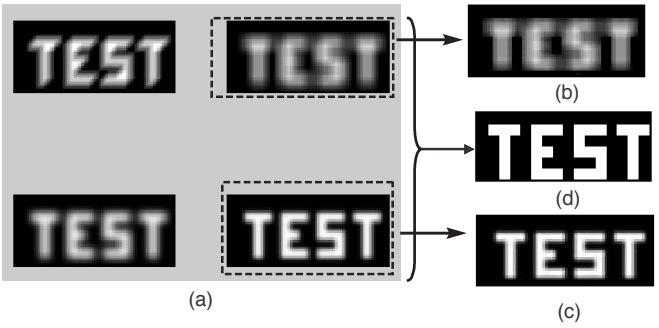

Fig. 1. (a) Set of degraded images used for MC deconvolution and altered by PSFs of size 7×7, (b)-(c) Restored image using a mono-channel deconvolution technique, (d) Perfectly restored image in the noiseless case using the multichannel deconvolution technique described in this article.

gain that can be obtained by MC processing. This gain is due to the inherent diversity of multichannel systems where multiple replica of the same signal/image are observed through different (independent) channels. In that case, if a part of the original information is lost (degraded) in one of the observed images, it can be retrieved from the other observed images upon certain diversity conditions. More precisely, this is possible when the same image distortion does not occur on

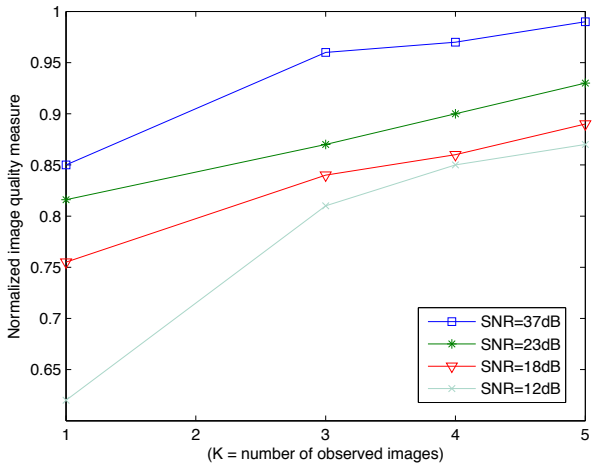

Fig. 2. Evolution of the restored image quality (using the PSF identification method followed by TV-based restoration) versus the number of observed images (PSFs) for different SNR values: Cameraman image.

all the observed images simultaneously. Mathematically, this is expressed in the condition that the spectral transforms of the PSFs do not share common zeros[1]. Indeed, a PSF's zero represents roughly a "fading" around a particular frequency point and hence common zeros represent the situation where the same fading occurs on all channels simultaneously. In the presence of noise, perfect reconstruction is not possible but the diversity gain provides significant improvement in the restored image quality. This is illustrated by figure 2 where we plot the restored image quality evaluated by the objective measure proposed in [19] versus the number of observed images (channels). In the mono-channel case, the restoration method used is the one introduced in [18]. For the MC case, we use the restoration method with the total variation approach (section VI). One can observe that the gain increases in terms of image restoration quality when using the MC processing. Furthermore, this gain is obtained with a relatively small number of independent PSFs (3 to 4 depending on the SNR level) which limits the extra computational burden of MC processing.

III. Problem Statement

A. Notations

It is assumed that a single image passes through $K > 2$ independent channels and hence K different noisy blurred images are observed. Each channel corresponds to a degrading filter. The notations used are:
- $\mathcal{F}$ the original image of size $m_f \times n_f$.
- $\mathcal{G}_1, \ldots, \mathcal{G}_K$ the K output images each of size $m_g \times n_g$.
- $\mathcal{H}_1, \ldots, \mathcal{H}_K$ the K point spread functions (PSFs) each of size $m_h \times n_h$ and $\mathbf{h}_1, \ldots, \mathbf{h}_K$ their row-wise vectorized versions. We denote by $\mathbf{h} = [\mathbf{h}_1^T, \ldots, \mathbf{h}_K^T]^T$ the vector of all PSF parameters. To satisfy the diversity condition, the PSF functions are assumed to have no common zeros, i.e. the

[1]Note that this condition can be met only if $K > 2$ different PSFs (channels) are available.

polynomials

$$\mathbf{H}_k(z_1,z_2)\overset{\triangle}{=}\sum_{i=0}^{m_h-1}\sum_{j=0}^{n_h-1}\mathcal{H}_k(i,j)z_1^{-i}z_2^{-j},\quad k=1,\ldots,K$$

are strongly co-prime.
- $\mathcal{N}_1,\ldots,\mathcal{N}_K$ the additive noise in each channel.
For the seek of notational simplicity, we adopt here a 'causal' representation of the considered filters so that the system model can be written as: for $k=1\ldots K$,

$$\mathcal{G}_k(m,n)=\sum_{l_1=0}^{m_h-1}\sum_{l_2=0}^{n_h-1}\mathcal{H}_k(l_1,l_2)\mathcal{F}(m-l_1,n-l_2)+\mathcal{N}_k(m,n).$$

In the sequel, the images and impulse responses will be processed in a vectorized, windowed form of size $m_w\times n_w$. Hence, we denote by $\mathbf{g}_k(m,n)$ the data vector corresponding to a window of the k^{th} image where the last pixel is indexed by (m,n), i.e. the right bottom pixel.

$$\begin{aligned}\mathbf{g}_k(m,n) &= [\mathcal{G}_k(m,n),\ldots,\mathcal{G}_k(m,n-n_w+1),\ldots,\\ &\qquad \mathcal{G}_k(m-m_w+1,n-n_w+1)]^T.\end{aligned}\tag{1}$$

In order to exploit the diversity and the redundancy offered by the multiple observations of $\mathcal{F}$, we deal simultaneously with all observed images by merging them into a single observation vector:

$$\mathbf{g}(m,n)=[\mathbf{g}_1^T(m,n),\ldots,\mathbf{g}_K^T(m,n)]^T=\mathbf{H}\mathbf{f}(m,n)+\mathbf{n}(m,n)\tag{2}$$

where $\mathbf{f}(m,n)$ is an $(m_w+m_h-1)(n_w+n_h-1)\times 1$ vector given by:

$$\begin{aligned}\mathbf{f}(m,n) &= [\mathcal{F}(m,n),\ldots,\mathcal{F}(m,n-n_w-n_h+1),\ldots,\\ &\qquad \mathcal{F}(m-m_w-m_h+1,n-n_w-n_h+1)]^T\end{aligned}$$

and $\mathbf{H}=\left[\mathbf{H}_1^T,\ldots,\mathbf{H}_K^T\right]^T$, $\mathbf{H}_k$ being the filter matrix associated to $\mathcal{H}_k$ given by :

$$\mathbf{H}_i=\begin{bmatrix}\mathbf{H}_i(0) & \ldots & \mathbf{H}_i(m_h-1) & & 0\\ & \ddots & & \ddots & \\ 0 & & \mathbf{H}_i(0) & \ldots & \mathbf{H}_i(m_h-1)\end{bmatrix}\tag{3}$$

with m_w blocks in the row direction and m_w+m_h-1 blocks in the column direction and

$$\mathbf{H}_i(n)=\begin{bmatrix}\mathcal{H}_i(n,0) & \ldots & \mathcal{H}_i(n,n_h-1) & & 0\\ & \ddots & & \ddots & \\ 0 & & \mathcal{H}_i(n,0) & \ldots & \mathcal{H}_i(n,n_h-1)\end{bmatrix}\tag{4}$$

of size $n_w\times(n_w+n_h-1)$.

B. Objectives

The ultimate goal is to restore the original image in a satisfactory way even in 'severe' observation conditions. In practice, the original image as well as the degrading filters are totally unknown. So that, our restoration procedure is totally blind. To tackle this problem two types of solutions are proposed. The direct image restoration technique [20] and the indirect one, that first estimates the unknown PSFs and then restores the original image in a non blind way (i.e. using the previously estimated PSFs) [12].

1) Direct restoration: Our objective here is to directly restore the original image using only its degraded observed versions. More precisely, we search for a unique equalizer or inverse filter which, applied to the set of observations, allows us to restore the original image. We pay a particular attention to the robustness against additive noise by including in the estimation criterion of the inverse filter an additional term that controls and limits the noise effect.

2) Restoration via PSF identification: Our objective here is to, first identify the PSF function and then inverse it in order to restore the original image. In the noisy case, the filter response inversion leads to noise amplification and hence we propose to add a regularization term in order to reduce this undesired effect. For that, we use the Total Variation (TV) constraint of the restored image as a regularization criterion. In the following, we deal with the direct restoration approach in section IV and with the indirect one in section VI. The PSF estimation methods are considered in section V.

IV. Regularized Mutually Referenced Equalizers (R-MRE)

In this section, we introduce our first image restoration method using the direct estimation of the inverse filters. These filters are estimated by MRE method in [17]. We propose some improvements in terms of computational cost and robustness against additive noise as shown below.

A. MRE method: review and improvements

We search, here, for the restoration filter denoted $\mathcal{E}$ which, applied to the K observed images, provides us with an estimate of the original image. This $\mathcal{E}$ is a multichannel 2D filter of size (Km_e,Kn_e). This filter exists under the following assumptions: (i) the PSFs have no common zeros (see [20] for more details) and (ii) the filter matrix has full column-rank. More precisely, it is proved in [17] that the channel matrix $\mathbf{H}$ is left invertible if:

$$Km_en_e\geq(m_h+m_e-1)(n_h+n_e-1).\tag{5}$$

When both conditions are satisfied, there exists a set of equalizers $\mathcal{E}_1,\ldots,\mathcal{E}_d$ each of them allowing us to restore the original image with a specific spatial shift $(m_d,\ n_d)$. Note that there exists an infinity of equalizers of different sizes (an infinity of couple (m_e,n_e)) that satisfy the condition in equation (5). Hence, when (m_e,n_e) is fixed, the original image is estimated up to a certain constant factor and a certain spatial shift. The principle of mutually referenced equalizers is as follows: suppose we have computed two equalizers $\mathcal{E}_i$ and $\mathcal{E}_j$ inducing the spatial shift (m_i,n_i) and (m_j,n_j) respectively:

$$\sum_{k=1}^{K}\mathcal{E}_{i,k}*\mathcal{G}_k(m,n)=\alpha\mathcal{F}(m-m_i,n-n_i),\ \forall\ (m,n)\tag{6}$$

$$\sum_{k=1}^{K}\mathcal{E}_{j,k}*\mathcal{G}_k(m,n)=\alpha\mathcal{F}(m-m_j,n-n_j),\ \forall\ (m,n)\tag{7}$$

where $*$ denotes the 2D convolution, α is a given positive scalar and $\mathcal{E}_i\overset{\triangle}{=}[\mathcal{E}_{i,1},\ldots,\mathcal{E}_{i,K}]$, $\mathcal{E}_{i,k}$ being the 2D filter of size

(m_e, n_e) applied to the k^{th} observed image.
In the noiseless case, if we apply the equalizer $\mathcal{E}_i$ to $\mathcal{G}(m - m_j, n - n_j)$ and the equalizer $\mathcal{E}_j$ to $\mathcal{G}(m - m_i, n - n_i)$ we obtain exactly the same windowed area of the original image:

$$\sum_{k=1}^{K} \mathcal{E}_{j,k} * \mathcal{G}_k(m - m_i, n - n_i) = \sum_{k=1}^{K} \mathcal{E}_{i,k} * \mathcal{G}_k(m - m_j, n - n_j). \quad (8)$$

In the original MRE method, it was shown that solving equation (8) for all equalizers inducing a spatial shift in the interval $[0, \ldots, m_e + m_h - 1] \times [0, \ldots, n_e + n_h - 1]$ leads to the computation of a set of equalizers which perfectly restore the original image in the noiseless case. This solution presents a major drawback: it requires the computation of a large number of equalizers (exactly $(m_e + m_h)(n_e + n_h)$ equalizers) and hence it is computationally expensive. In [17] and [21] it is shown that we can reduce the number of equalizers to be estimated and, consequently, the computational cost of this solution. More precisely, it was proved that only 2 extremal equalizers $\mathcal{E}_1, \mathcal{E}_2$ corresponding to the extremal spatial shifts $(m_1, n_1) = (0, 0)$ and $(m_2, n_2) = (m_e + m_h - 1, n_e + n_h - 1)$ are sufficient for perfect image restoration. In practice, these shifts do not appear to perform good restoration quality due to the artefacts appearing in the boundaries of the restored image. Therefore, we propose to use a third equalizer corresponding to the median shift $(m_3, n_3) = (\lceil \frac{m_2}{2} \rceil, \lceil \frac{n_2}{2} \rceil)$ where $\lceil . \rceil$ denotes the integer part. Solving equation (8) for equalizers $\mathcal{E}_1$, $\mathcal{E}_2$ and $\mathcal{E}_3$, consists in solving the following set of linear equations:

$$\begin{aligned}
&\sum_{k=1}^{K} \mathcal{E}_{2,k} * \mathcal{G}_k(m - m_1, n - n_1) = \sum_{k=1}^{K} \mathcal{E}_{1,k} * \mathcal{G}_k(m - m_2, n - n_2) \\
&\sum_{k=1}^{K} \mathcal{E}_{3,k} * \mathcal{G}_k(m - m_2, n - n_2) = \sum_{k=1}^{K} \mathcal{E}_{2,k} * \mathcal{G}_k(m - m_3, n - n_3). \\
&\sum_{k=1}^{K} \mathcal{E}_{1,k} * \mathcal{G}_k(m - m_3, n - n_3) = \sum_{k=1}^{K} \mathcal{E}_{3,k} * \mathcal{G}_k(m - m_1, n - n_1)
\end{aligned} \quad (9)$$

In practice, in order to take into account the additive noise, this set of equations is solved in the least squares sense leading to a quadratic form that can be written as follows:

$$J_{MRE}(\mathbf{e}) = \mathbf{e}^T \mathbf{Q}_{MRE} \mathbf{e} \quad (10)$$

where $\mathbf{e} = [\mathbf{e}_1^T, \mathbf{e}_2^T, \mathbf{e}_3^T]^T$, $\mathbf{e}_i = [\mathbf{e}_{i,1}^T, \ldots, \mathbf{e}_{i,K}^T]^T$ and $\mathbf{e}_{i,k}$ is the row-wise vectorized version of $\mathcal{E}_{i,k}$. The quadratic form $\mathbf{Q}_{MRE}$ is given by:

$$\mathbf{Q}_{MRE} = \begin{bmatrix} \mathbf{R}_{22} + \mathbf{R}_{33} & -\mathbf{R}_{21} & -\mathbf{R}_{31} \\ -\mathbf{R}_{12} & \mathbf{R}_{11} + \mathbf{R}_{33} & -\mathbf{R}_{32} \\ -\mathbf{R}_{13} & -\mathbf{R}_{23} & \mathbf{R}_{11} + \mathbf{R}_{22} \end{bmatrix}$$

where $\mathbf{R}_{ij} = \sum_{(m,n)} \mathbf{g}(m - m_i, n - n_i)\mathbf{g}^T(m - m_j, n - n_j)$, $(i, j) \in \{1, 2, 3\}$ and $\mathbf{g}$ is the vector defined in equation (2) with $(m_w, n_w) = (m_e, n_e)$. $\mathbf{Q}_{MRE}$ matrix is singular and its rank depends on the equalizer size (m_e, n_e), therefore, $J_{MRE}(\mathbf{e})$ criterion must be minimized under unit-norm constraint.

B. Regularized MRE method

In the noisy case, the MRE algorithm fails in restoring efficiently the image. This is due to the ill-conditioned filter matrix whose inversion leads to noise amplification. In order to come through this difficulty, we propose, here, to combine the MRE criterion in equation (10) with a regularization technique inspired from [22] and adapted to the multichannel framework. In fact, the noise amplification is due to the largest singular values of the Inverse Filter Matrix (IFM). Therefore, our regularization technique simply consists in the truncation of the largest singular values of the IFM. This truncation is realized through an adaptive thresholding technique which is explained below. Now, to reduce the computational cost of the desired eigenvalues, we exploit the Toeplitz structure and the large dimension of the inverse filter matrix in such a way to approximate it by a block circulant matrix [23] whose eigenvalues can be computed by means of Fourier transform [24].
In this work, we choose $\mathcal{E}_3$ among the MRE equalizers to restore the original image as it provides the best restoration performance compared to extremal shift equalizers $\mathcal{E}_1$ and $\mathcal{E}_2$ as mentioned previously. Let us write this equalizer as:

$$\mathcal{E}_3 \triangleq [\mathcal{E}_{3,1}, \ldots, \mathcal{E}_{3,K}] \quad (11)$$

and let $\mathbf{E}_k$ be the IFM associated with $\mathcal{E}_{3,k}$ and defined as in equations (3) and (4). Since $\mathbf{E}_k$ is a large block Toeplitz matrix with Toeplitz blocks, it can be approximated by a large block circulant matrix $\tilde{\mathbf{E}}_k$ with circulant blocks. This approximation leads to the following estimation:

$$\sum_{k=1}^{K} \tilde{\mathbf{E}}_k \mathbf{g}_k \approx \mathbf{f}_3 \quad (12)$$

where $\mathbf{f}_3$ denotes the original image in vector form shifted by (m_3, n_3): $\mathbf{f}_3 = [\mathcal{F}(m_f - m_3, n_f - n_3), \ldots, \mathcal{F}(m_f - m_3, 1), \ldots, \mathcal{F}(1, 1)]^T$. $\mathbf{g}_k$ denotes the k^{th} observed image in vector form: $\mathbf{g}_k = [\mathcal{G}_k(m_g, n_g), \ldots, \mathcal{G}_k(1, 1)]^T$. Let define $\tilde{\mathbf{E}}$ as a block circulant matrix with circulant blocks $\tilde{\mathbf{E}}_k$: $\tilde{\mathbf{E}} = \begin{bmatrix} \tilde{\mathbf{E}}_1 & \tilde{\mathbf{E}}_2 & \ldots & \tilde{\mathbf{E}}_K \\ \tilde{\mathbf{E}}_K & \tilde{\mathbf{E}}_1 & \ldots & \tilde{\mathbf{E}}_{K-1} \\ \vdots & & & \\ \tilde{\mathbf{E}}_2 & \tilde{\mathbf{E}}_3 & \ldots & \tilde{\mathbf{E}}_1 \end{bmatrix}$. Eq. (12) become: $\tilde{\mathbf{E}} \begin{bmatrix} \mathbf{g}_1 \\ \vdots \\ \mathbf{g}_K \end{bmatrix} \approx \begin{bmatrix} \mathbf{f}_3 \\ \star \\ \star \end{bmatrix}$.

As mentioned in section IV, we propose to truncate the largest eigenvalues of $\tilde{\mathbf{E}}$ to avoid noise amplification when restoring the original image. A well known property of circulant matrices is that their eigenvalues can be expressed as a function of the elements of the first column. This property can be extended to block circulant matrices by considering the first column of each column block. Since $\tilde{\mathbf{E}}$ is a block circulant matrix with circulant blocks $\tilde{\mathbf{E}}_k$, it can be proved [23] that its eigenvalues are given by:

$$\mathbf{u} = [u_1, \ldots, u_{Kn}]^T = \mathbf{M}\mathbf{e} \quad (13)$$

where $\mathbf{u}$ is a vector containing the eigenvalues of $\tilde{\mathbf{E}}$, $\mathbf{M}$ is a known sparse matrix and n is the number of pixels in the restored image. In order to truncate the largest eigenvalues of $\tilde{\mathbf{E}}$, we apply a non-linear filter represented by a projection matrix $\mathbf{B}$. Let $\tilde{\mathbf{u}} = \mathbf{B}\mathbf{u}$ where $\mathbf{B} = diag(b_i)$ and

$$b_i = \begin{cases} 1, & if \quad \mid u_i \mid \leq \tau \\ 0, & otherwise \end{cases} \quad (14)$$

τ is a predetermined threshold. Here, we choose

$$\tau = c. \max_i(|u_i|) \quad (15)$$

where c is a chosen scalar in the range $[0 \quad 1]$ whose value depends on the image type. Let $\mathbf{v} = \mathbf{u} - \tilde{\mathbf{u}}$ be the error between the original vector of eigenvalues and the truncated one, $\mathbf{v} =$

$(\mathbf{I}-\mathbf{B})\mathbf{u}$. The regularized MRE criterion can be then expressed as:

$$\begin{aligned} J_{reg}(\mathbf{e}) &= J_{MRE}(\mathbf{e}) + \mu\|\mathbf{v}\|^2 \\ &= \mathbf{e}^T\mathbf{Q}_{MRE}\mathbf{e} + \mu\|(\mathbf{I}-\mathbf{B})\mathbf{M}\mathbf{e}\|^2 \\ &= \mathbf{e}^T\mathbf{Q}_{reg}\mathbf{e}, \end{aligned} \tag{16}$$

with

$$\mathbf{Q}_{reg} = \mathbf{Q}_{MRE} + \mu\mathbf{M}^T(\mathbf{I}-\mathbf{B})\mathbf{M}, \quad \text{and} \tag{17}$$

$$\mathbf{e} = [\mathbf{e}_1, \mathbf{e}_2, \mathbf{e}_3]. \tag{18}$$

In equation (18), μ represents a scalar factor that controls the amount of regularization we would like to incorporate into the MRE criterion. Note that J_{reg} is a non linear criterion since $\mathbf{B}$ depends non linearly on $\mathbf{e}$. However, once $\mathbf{B}$ is fixed, J_{reg} becomes quadratic and it can be easily solved by means of a classical minimization algorithm. Here, we use a two step optimization procedure. First, we compute the MRE equalizer $\mathbf{e}_{MRE}$ that minimizes the MRE criterion without regularization. Then the equalizer $\mathbf{e}_{MRE}$ is used to fix the thresholding matrix $\mathbf{B}$. Once $\mathbf{B}$ fixed, the R-MRE criterion J_{reg} becomes quadratic and, hence, can be minimized using a classical optimization scheme. Note that the solution set of the R-MRE criterion contains the desired filters but also, undesired 'blocking' filters $\bar{\mathcal{E}}$ (denoted $\bar{\mathbf{e}}$ in vector form) that satisfy in the noiseless case:

$$\bar{\mathbf{e}}^T\mathbf{g}(m,n) = 0 \quad \forall(m,n). \tag{19}$$

For example, the filter $\bar{\mathcal{E}}$ given by $\bar{\mathcal{E}}_1 = -\mathcal{H}_2$, $\bar{\mathcal{E}}_2 = \mathcal{H}_1$ and $\bar{\mathcal{E}}_k = 0$, $\forall k = 3, \ldots, K$, is a blocking filter as it satisfies $\sum_{k=1}^{K} \bar{\mathcal{E}}_k * \mathcal{G}_k(m,n) = 0$. Consequently, we search for a solution that minimizes the criterion (16) and maximizes the restored image energy. Indeed, a blocking filter output is given by noise term only while the desired restoration filter would provide us with an approximate version of the original image hat is assumed to have a much larger energy than noise. To achieve the previous objective, we simply constrain this energy to be unitary, i.e, we solve criterion (16) under the following energy constraint:

$$\mathbf{e}_{reg}^T(\mathbf{I}_3 \otimes \mathbf{R}_{11})\mathbf{e}_{reg} = 1 \tag{20}$$

where $\otimes$ denotes the matrix Kronecker product. This is equivalent to minimizing the Rayleigh quotient:

$$min \frac{\mathbf{e}_{reg}^T\mathbf{Q}_{reg}\mathbf{e}_{reg}}{\mathbf{e}_{reg}^T(\mathbf{I}_3 \otimes \mathbf{R}_{11})\mathbf{e}_{reg}} \tag{21}$$

which solution is given by the principal generalized eigenvector of $((\mathbf{I}_3 \otimes \mathbf{R}_{11}), \mathbf{Q}_{reg})$.

V. PSF Blind Identification Techniques

The second approach to perform MBD consists in first identifying the degradation filters and then inverting them in order to restore the original image. In this section we are interested in identifying the blur functions in each channel that would be used later for image restoration by means of TV−based regularization technique. More precisely, we first carry out a comparative study of several existing deterministic techniques for multichannel blind image identification identification techniques, namely, the subspace method (SS), the minimum noise subspace method (MNS) and the cross-relation (CR) method. These methods are quite similar in the principle, in fact they compute some 'correlation' and 'redundance' between the different acquisitions in order to retrieve the degrading filters. Then, we propose a new identification algorithm based on a smoothing least squares technique. In this section, we present the principle and the algorithm of each method before comparing their performance using computer simulation experiments.

A. The subspace method (SS)

The SS method for image restoration was first introduced in [25]. It exploits the fact that, in the noiseless case, all vectors $\mathbf{g}(m,n)$ are in the subspace scanned by the column vectors of $\mathbf{H}$ (the image data subspace). Hence, we can estimate the column range space of $\mathbf{H}$ ($Range(\mathbf{H})$) from the observed data. In practice, in order to take into account the additive noise, we estimate $Range(\mathbf{H})$ as the subspace $\mathbf{U}_s$ spanned by the principal eigenvectors of $\mathbf{R}_{11}$, the covariance matrix of $\mathbf{g}$. On the other hand, it is shown in [25], that $Range(\mathbf{H})$ characterizes uniquely the parameter vector $\mathbf{h}$ (up to a constant factor)[2]. As a consequence, we can estimate the unknown channel parameters $\mathbf{h}$ by fitting the range space of $\mathbf{H}$ to the image data subspace measured from the observation. The best fit is reached when $\mathbf{H}$ is preserved (unaltered) by orthogonal projection onto $Range(\mathbf{U}_s)$. This can be performed by minimizing the least squares criterion:

$$\mathbf{H}^T(\mathbf{I}-\mathbf{U}_s\mathbf{U}_s^T)\mathbf{H} = \mathbf{H}^T\mathbf{U}_n\mathbf{U}_n^T\mathbf{H} = \left\|\mathbf{U}_n^T\mathbf{H}\right\|^2 \tag{22}$$

where $\mathbf{U}_n = [\mathbf{u}_1, \ldots, \mathbf{u}_{d_n}]$ represents the matrix of minor (least) eigenvectors of $\mathbf{R}_{11}$ referred to as the noise subspace. Note that $\mathbf{U} = [\mathbf{U}_s\ \mathbf{U}_n]$ is unitary and hence $\mathbf{I} - \mathbf{U}_s\mathbf{U}_s^T = \mathbf{U}_n\mathbf{U}_n^T$. As $\mathbf{H}$ is a linear function of $\mathbf{h}$, the criterion in equation (22) is a quadratic form of $\mathbf{h}$ that can be written as:

$$\left\|\mathbf{U}_n^T\mathbf{H}\right\|^2 = \sum_{i=1}^{d_n}\left\|\mathbf{u}_i^T\mathbf{H}\right\|^2 = \mathbf{h}^T\mathbf{Q}_{SS}\mathbf{h} \tag{23}$$

where $\mathbf{Q}_{SS} = \sum_{i=1}^{d_n}\mathcal{U}_i\mathcal{U}_i^T$ is obtained from $\mathbf{U}_n$ by using the relation $\mathbf{u}_i^T\mathbf{H} = \mathbf{h}^T\mathcal{U}_i$ where $\mathcal{U}_i$ is a function of $\mathbf{u}_i$ that can be obtained by straightforward algebraic manipulations. The latter criterion is minimized under unit-norm constraint, i.e $\|\mathbf{h}\| = 1$, to avoid the trivial solution $\mathbf{h} = 0$, so that $\mathbf{h}$ corresponds to the least eigenvector of $\mathbf{Q}_{SS}$. The SS algorithm is summarized in Table I.

B. Minimum Noise Subspace Method (MNS)

The MNS method is a simplified version of the SS one. It is based on the same principle but it does not use all the noise subspace but a minimum number of noise space vectors. Indeed, it is shown in [26], that, instead of using the d_n noise vectors ($d_n >> 1$), only $(K-1)$ properly chosen noise space vectors are sufficient to guarantee the uniqueness of the solution of equation (23) (up to a scalar factor). To estimate the noise space vectors, we consider $K-1$ image pairs that form a tree structure. For each pair (i_1, i_2), we

[2]The constant factor is an inherent ambiguity in blind system identification as the exchange of a scalar between $\mathbf{H}$ and $\mathbf{f}$ does not affect the observation, i.e $\mathbf{g} = \mathbf{H}\mathbf{f} = \alpha\mathbf{H}.(\frac{1}{\alpha}\mathbf{f})$.

1. For $m_w \geq m_h$ and $n_w \geq n_h$; construct a data matrix

$$\mathbf{D} = [\mathbf{g}(m_w, n_w),\ \mathbf{g}(m_w, n_w + 1), \ldots, \mathbf{g}(m_g, n_g)].$$

2. Compute the estimate of the auto-covariance matrix

$$\hat{\mathbf{R}}_{11} = \frac{1}{m_g n_g}\mathbf{D}\mathbf{D}^T.$$

3. Compute the eigen-decomposition of $\hat{\mathbf{R}}_{11}$ and extract the d_n eigenvectors that are in the noise subspace ($d_n = Km_w n_w - (m_h + m_w - 1)(n_h + n_w - 1)$).
4. Construct $\mathbf{Q}_{SS}$ from $\mathbf{U}_n$ and compute $\mathbf{h}$ as the eigenvector corresponding to the smallest eigenvalue of $\mathbf{Q}_{SS}$.

TABLE I
THE SS ALGORITHM.

estimate the least eigenvector of the covariance matrix of $\left[\mathbf{g}_{i_1}^T(m,n),\ \mathbf{g}_{i_2}^T(m,n)^T\right]^T$ which is zero padded (as shown in Table II) to form a noise space vector. By doing so, we avoid the computationally expensive eigen-decomposition of $\mathbf{R}_{11}$ required in the SS method. Moreover, the $(K-1)$ noise space vectors can be computed in a parallel scheme if a parallel architecture is available. These $(K-1)$ noise space vectors, $\mathbf{v}_1, \ldots, \mathbf{v}_{K-1}$, are then used in equation (23) to form the LS criterion $\sum_{i=1}^{K-1} \|\mathbf{v}_i^T\mathbf{H}\|^2 = \mathbf{h}^T(\sum_{i=1}^{K-1}\mathcal{V}_i\mathcal{V}_i^T)\mathbf{h} = \mathbf{h}^T\mathbf{Q}_{MNS}\mathbf{h}$ that is solved similarly to the SS method, under unit-norm constraint. The MNS algorithm is summarized in Table II. In

1. Select $K-1$ distinct pairs that form a tree pattern from K observed images.
2. For each pair $\mathbf{i} = (i_1, i_2)$, construct the data matrix and its corresponding covariance matrix:

$$\mathbf{D}_i = \begin{bmatrix} \mathbf{g}_{i_1}(m_w, n_w) & \cdots & \mathbf{g}_{i_1}(m_g, n_g) \\ \mathbf{g}_{i_2}(m_w, n_w) & \cdots & \mathbf{g}_{i_2}(m_g, n_g) \end{bmatrix}$$

and $\hat{\mathbf{R}}_i = \frac{1}{m_g n_g}\mathbf{D}_i\mathbf{D}_i^T$
3. Compute the least dominant eigenvector of $\hat{\mathbf{R}}_i$:

$$\mathbf{v}^{(i_1,i_2)} = \begin{bmatrix} \mathbf{v}^{(i_1,i_2)}(1) \\ \mathbf{v}^{(i_1,i_2)}(2) \end{bmatrix}.$$

4. Construct a zero-padded vector $\mathbf{v}_i$ consisting of K blocks of size $m_w n_w$ each. Place $\mathbf{v}^{(i_1,i_2)}(1)$ as its i_1^{th} block, $\mathbf{v}^{(i_1,i_2)}(2)$ in the i_2^{th} block and zeros elsewhere.
5. Construct $\mathbf{Q}_{MNS} = \sum_{i=1}^{K-1}\mathcal{V}_i\mathcal{V}_i^T$ and compute $\mathbf{h}$ as the eigenvector corresponding to the smallest eigenvalue of $\mathbf{Q}_{MNS}$.

TABLE II
THE MNS ALGORITHM.

the original MNS method, some observed images are used more than others, depending on the chosen set of image couples. This might lead to poor estimation performance if the system outputs that were chosen correspond to the 'worst observed images'. This raises the problem of the best choice of the appropriate set of outputs and motivates the development of a Symmetric MNS method (SMNS). In SMNS technique we guarantee a certain symmetry in the choice of the set of observed image couples. For instance, for $K = 4$ channels, we use the following channel couples: (1,2), (2,3), (3,4), (4,1). This choice makes the SMNS method more robust than MNS one in terms of estimation accuracy. Hence, SMNS algorithm is the same as the MNS except for the fact that we use K pairs of observed images: $(1,2), (2,3), \ldots, (K-1,K), (K,1)$,

1. For all (m,n), compute $\mathbf{\Psi}(m,n)$.
2. Compute the quadratic form

$$\mathbf{Q}_{CR} = \sum_{m,n}\mathbf{\Psi}^T(m,n)\mathbf{\Psi}(m,n).$$

3. Compute $\mathbf{h}$ as the least dominant eigenvector of $\mathbf{Q}_{CR}$.

TABLE III
THE CR ALGORITHM.

instead of an ad-hoc choice of $(K-1)$ pairs forming a tree structure.

C. Cross Relation method (CR)

The CR method was first introduced in [27]. It is based on the commutativity of the convolution operator. In fact, in the noiseless case, we observe that: $\mathcal{H}_i * \mathcal{G}_j(m,n) = \mathcal{H}_j * \mathcal{G}_i(m,n)$. Therefore,

$$[\mathbf{g}_i(m,n)^T, \quad -\mathbf{g}_j(m,n)^T]\begin{bmatrix}\mathbf{h}_j \\ \mathbf{h}_i\end{bmatrix} = 0, \quad \forall (i,j).$$

We can write this relation for any pair of channels. We have a total of $\frac{K(K-1)}{2}$ pairwise equations corresponding to:

$$\mathbf{\Psi}(m,n)\mathbf{h} = 0, \quad \forall\ (m,n) \tag{24}$$

where

$$\mathbf{\Psi}(m,n) = \begin{bmatrix} \mathbf{\Psi}_1(m,n) \\ \vdots \\ \mathbf{\Psi}_{K-1}(m,n) \end{bmatrix}$$

$$\mathbf{\Psi}_k(m,n) = \begin{bmatrix} 0 & \ldots & 0 & \mathbf{g}_{k+1}^T & -\mathbf{g}_k^T & & 0 \\ \vdots & \ddots & \vdots & \vdots & & \ddots & \\ 0 & \ldots & 0 & \mathbf{g}_K^T & 0 & & -\mathbf{g}_k^T \end{bmatrix}.$$

Inversely, it is shown in [28] that equation (24) characterizes uniquely -up to a constant factor- the unknown channel parameter vector $\mathbf{h}$. Hence, the CR method consists in estimating $\mathbf{h}$ by solving equation (24) in the LS sense:

$$\min_{\mathbf{h}} \sum_{m,n}\|\mathbf{\Psi}(m,n)\mathbf{h}\|^2 = \mathbf{h}^T\mathbf{Q}_{CR}\mathbf{h}.$$

Again, the solution of the above LS criterion under unit-norm constraint of $\mathbf{h}$, is given by the least eigenvector of $\mathbf{Q}_{CR}$. This method presents a real computational gain as it requires only one eigenvector computation whereas the other methods require two or more eigen-decompositions. Moreover, we can further reduce the computational cost by choosing, as for the MNS and SMNS methods, only $(K-1)$ or K pairs of cross-relations. The CR algorithm is summarized on Table III.

D. Least Squares Smoothing Method (LSS)

The LSS method is an estimation technique that exploits the isomorphism between the input and the output spaces. LSS has been introduced in [13] in the 1D case. We propose, here, to generalize it for the first time to the 2D signals. Indeed, in the noiseless case, one can write the data matrix as follows:

$$\mathbf{D}_{LSS} \triangleq [\mathbf{g}(2m_h+1, 2n_h+1), \ldots, \mathbf{g}(m_g - m_h, n_g - n_h)] \tag{25}$$

$$= \mathbf{H}\mathbf{F} \tag{26}$$

with,

$$\mathbf{F} = [\mathbf{f}(2m_h+1, 2n_h+1), \ldots, \mathbf{f}(m_g - m_h, n_g - n_h)].$$

Since $\mathbf{H}$ is full column rank, the row space of $\mathbf{D}_{LSS}$ (output space) coincides with the row space of $\mathbf{F}$ (input space). This allows us to construct appropriate projection subspaces using only observed data. More precisely, let S_i be a row subspace that contains all rows of $\mathbf{F}$ except the i^{th} one (referred to as $\mathbf{F}_{i,:}$). In order to construct S_i, first, note that each column of matrix $\mathbf{F}$ consists in $n_b = n_h + n_w - 1$ blocks containing $n_c = m_h + m_w - 1$ elements each one. So that, each row index r in matrix $\mathbf{F}$ can be written as $r = kn_c + l$, $0 \leq k \leq n_b - 1$ and $1 \leq l \leq n_c$. Let i be the index of the row to be selected : $i = k_i n_c + l_i$. In order to extract the i^{th} row of matrix $\mathbf{F}$, we first eliminate the rows in all row blocks of $\mathbf{F}$ except those in blocks k_i, i.e. rows corresponding to blocks k in the range $[0,\ k_i - 1]$ and $[k_i + 1,\ n_b - 1]$. In our work, we consider $i = (m_h - 1)n_c + (n_h - 1)$, for which the previous row vectors belong to the subspace generated by the rows of $\mathbf{B}^r = [\mathbf{g}(1, n_h + 1), \ldots, \mathbf{g}(m_g - 3m_h, n_g - 2n_h)]$ and $\mathbf{B}^c = [\mathbf{g}(m_h + 1, 1), \ldots, \mathbf{g}(m_g - 2m_h, n_g - 3n_h)]$ respectively. Then, we eliminate the rows in the same block as row i, i.e. rows in the k_i^{th} block corresponding to indices l in the range $[1,\ l_i - 1]$ and $[l_i + 1,\ n_c]$ (for $i = (m_h - 1)n_c + (n_h - 1)$, $k_i = m_h - 1$ and $l_i = n_h - 1$). These rows live in the subspace spanned by the row vectors of $\mathbf{F}^r = [\mathbf{g}(2m_h + 1, n_h + 1), \ldots, \mathbf{g}(m_g - m_h, n_g - 2n_h)]$ and $\mathbf{F}^c = [\mathbf{g}(m_h + 1, 2n_h + 1), \ldots, \mathbf{g}(m_g - 2m_h, n_g - n_h)]$ respectively. Finally, S_i is constructed from the row space generated by $S = [\mathbf{B}^{rT},\ \mathbf{B}^{cT},\ \mathbf{F}^{rT},\ \mathbf{F}^{cT}]^T$. This subspace will be used to project the data matrix $\mathbf{D}$. In practice, to take into account additive noise, the desired row space is estimated from the principal right singular vectors of S. The projection error of $\mathbf{D}_{LSS}$ onto this row space allows us to extract the i^{th} column vector $\mathbf{H}_{:,i}$ of $\mathbf{H}$, i.e.

$$\mathbf{E}_{LSS} = \mathbf{D}_{LSS} - \mathbf{D}_{LSS}|_{S_i} = \mathbf{H}_{:,i}\mathbf{F}_{i,:}|_{S_i},$$

where $\mathbf{E}_{LSS}$ is a rank one matrix with principal singular vector equal to $\mathbf{H}_{:,i}$ up to a scalar factor. By selecting a column vector of $\mathbf{H}$ that contains all channel coefficients, one can estimate the latter through the estimation of $\mathbf{H}_{:,i}$ as the principal left singular eigenvector of $\mathbf{E}_{LSS}$. Note that many columns of $\mathbf{H}$ contain all channel coefficients. Using equation (3), one can observe that the column blocks in the range $[m_h - 1,\ m_w - 1]$ contain all block matrices $\mathbf{H}_i(k),\ k = 0, \ldots, m_h - 1,\ i = 1, \ldots, K$. Similarly, equation (4) shows that the column vectors of $\mathbf{H}_i(n)$ in the range $[n_h - 1,\ n_w - 1]$ contain all the coefficients $\mathcal{H}_i(n, k),\ k = 0, \ldots, n_h - 1$. Consequently, the column index i should be in the set $\{kn_b + l,\ k \in [m_h - 1, \ldots, n_w - 1],\ l \in [n_h - 1, \ldots, n_w - 1]\}$ (which justifies the choice of $i = (m_h - 1)n_c + n_h - 1$) . The LSS algorithm is summarized in Table IV.

Remark: All the considered identification methods require the a-priori knowledge of the PSF size, i.e m_h and n_h. A main advantage of the LSS method is the possibility to relax this constraint in a joint channel parameter and channel size estimation framework. This implementation has already been considered in [13] in the 1D case and can be used in the 2D case as well.

1. Construct the data matrix:

$$\mathbf{D}_{LSS} = [\mathbf{g}(2m_h + 1, 2n_h + 1), \ldots, \mathbf{g}(m_g - m_h, n_g - n_h)]$$

2. Construct the projection matrix (matrix from which the subspace projection is computed):

$$S = [\mathbf{B}^{rT}, \mathbf{B}^{cT}, \mathbf{F}^{rT}, \mathbf{F}^{cT}]^T$$
$$\mathbf{B}^r = [\mathbf{g}(2m_h + 1, n_h + 1), \ldots, \mathbf{g}(m_g - m_h, n_g - 2n_h)]$$
$$\mathbf{B}^c = [\mathbf{g}(2m_h + 1, 3n_h + 1), \ldots, \mathbf{g}(m_g - m_h, n_g)]$$
$$\mathbf{F}^r = [\mathbf{g}(2m_h + 1, n_h + 1), \ldots, \mathbf{g}(m_g - m_h, n_g - 2n_h)]$$
$$\mathbf{F}^c = [\mathbf{g}(m_h + 1, 2n_h + 1), \ldots, \mathbf{g}(m_g - 2m_h, n_g - n_h)]$$

3. Compute the projection matrix $\mathcal{V}^T\mathcal{V}$ where $\mathcal{V}$ is the matrix of principal right singular vectors of S ($\mathcal{V}$ is of rank $(m_h + m_w - 1)(n_h + n_w - 1) + (m_w + m_h - 2) + (n_w + n_h - 2)$).
4. Compute $\mathbf{E}_{LSS}$ as the residue of orthogonal projection of $\mathbf{D}_{LSS}$ onto Range($\mathcal{V}$), i.e.

$$\mathbf{E}_{LSS} = (\mathbf{I} - \mathcal{V}^T\mathcal{V})\mathbf{D}_{LSS}.$$

5. Compute $\mathbf{H}_{:,i}$ ($i = (m_h - 1)n_c + (n_h - 1)$) as the principal left singular vector of $\mathbf{E}_{LSS}$.

TABLE IV
THE LSS ALGORITHM.

VI. IMAGE RESTORATION USING IDENTIFIED FILTERS

In this section, we are interested in a restoration technique which consists in retrieving the original image using both the set of observed images and the identified filters in section V. We propose to generalize the Total Variation (TV) method, first introduced in [29] in the monochannel case, to the multichannel case and to use it to control the noise amplification during the inverse filtering. To this end, we consider a regularized least squares criterion $T(\mathbf{f})$ given by:

$$T(\mathbf{f}) = \frac{1}{2}\sum_{k=1}^{K} \|\mathbf{H}_k\mathbf{f} - \mathbf{g}_k\|_2^2 + \lambda J_{TV}(\mathbf{f}). \tag{27}$$

$\lambda > 0$ is a scalar parameter that controls the amount of the desired regularization and hence measures the trade-off between a good fit and the regularity of the solution. $\mathbf{f}$ denotes the vectorized version of original image $\mathcal{F}$. $\mathbf{H}_k$ is the filter matrix associated to the k^{th} PSF estimate. $\mathbf{g}_k$ is the k^{th} observed image. $J_{TV}(\mathbf{f})$ is the well known TV of the original image which is expressed in the continuous 2D domain as [29]:

$$J_{TV}(f) = \int_{\Omega_f} \|\nabla f(x, y)\|_2 \ dxdy = \int_{\Omega_f} \sqrt{(\frac{\partial f}{\partial x})^2 + (\frac{\partial f}{\partial y})^2}\ dxdy. \tag{28}$$

where f represents a differentiable 2D function and Ω_f its spatial support. The minimization of the regularized least squares criterion (27) necessitates the derivation of $T(\mathbf{f})$ which raises the problem of differentiability of J_{TV}. In fact, $\|\nabla.\|_2$ is non-differentiable at zero point. Consequently, the TV term is approximated as follows [29]:

$$J_{TV,\beta}(f) = \int_{\Omega_f} \sqrt{(\frac{\partial f}{\partial x})^2 + (\frac{\partial f}{\partial y})^2 + \beta^2}\ dxdy. \tag{29}$$

where β is a small scalar parameter which allows to disturb the gradient value around zero point in order to guarantee its differentiability. In order to numerically estimate the derivative of $T(\mathbf{f})$, it is necessary to compute a discrete version of the TV term. Then, classical numerical algorithms, such as gradient descent optimization, could be used to solve criterion (27)

and estimate $\hat{\mathbf{f}}$ the desired solution. The discrete gradient of image $\mathbf{f}$ is expressed using derivative operators D^c and D^r in the column direction (c) and the row one (r), respectively. The expressions of the corresponding matrices $\mathbf{D}^c$ and $\mathbf{D}^r$ depend on the approximation technique adopted to compute the gradient [30]. These operators have the following matrix representation: $\mathbf{D}^{(c)} = \mathbf{I}_{m_f} \otimes \mathbf{D}^c$ and $\mathbf{D}^{(r)} = \mathbf{D}^r \otimes \mathbf{I}_{n_f}$ where $\otimes$ represents the Kronecker product. Several approximations can be used to compute this gradient. Here, we use the central derivative in the central part of the image and we consider the forward derivative on the image boundaries. Using these operators, the TV term can be expressed in the discrete form as:

$$J_{TV}(\mathbf{f}) = \sum_{s=1}^{m_f n_f} \psi_s = \sum_{s=1}^{m_f n_f} \sqrt{(u_s^2 + v_s^2 + \beta^2)} \tag{30}$$

where $u_s = (\mathbf{D}^{(c)}\mathbf{f})_s$ and $v_s = (\mathbf{D}^{(r)}\mathbf{f})_s$ represent the s^{th} element of vector $\mathbf{D}^{(c)}\mathbf{f}$ and $\mathbf{D}^{(r)}\mathbf{f}$, respectively.

Let f_i be an element of vector $\mathbf{f}$, computing the derivative of $T(\mathbf{f})$ with respect to f_i leads to:

$$\frac{\partial T(\mathbf{f})}{\partial f_i} = \sum_{k=1}^{K} (\mathbf{H}_k^T(\mathbf{H}_k\mathbf{f} - \mathbf{g}_k))_i + \lambda \sum_{s=1}^{m_f n_f} \frac{\partial \psi_s}{\partial f_i} \tag{31}$$

where,

$$\frac{\partial \psi_s}{\partial f_i} = \frac{\partial \psi_s}{\partial u_s}\frac{\partial u_s}{\partial f_i} + \frac{\partial \psi_s}{\partial v_s}\frac{\partial v_s}{\partial f_i} = D_{s,i}^{(c)}\frac{\partial u_s}{\partial f_i} + D_{s,i}^{(r)}\frac{\partial v_s}{\partial f_i} \tag{32}$$

where $D_{s,i}^{(c)}$ and $D_{s,i}^{(r)}$ represent the $(s,i)^{th}$ entries of matrices $\mathbf{D}^{(c)}$ and $\mathbf{D}^{(r)}$, respectively. The estimate of the original image $\hat{\mathbf{f}}$ satisfies:

$$\frac{\partial T(\hat{\mathbf{f}})}{\partial f_i} = 0, \ \forall i = 1, ..., m_f n_f. \tag{33}$$

When using numerical algorithms in order to solve equation (33), two difficulties are encountered: (i) the non-linearity of terms $\frac{\partial \psi_s}{\partial u_s}$ and $\frac{\partial \psi_s}{\partial v_s}$, (ii) the non-regularity of the desired solution. In fact, concerning point (ii), it is well know that the grey levels of a digital image present some jumps and steep gradients especially at edge locations. So, the solution of equation (33) must satisfy such properties. Numerical optimization algorithms such as Raphson-Newton suffer from local minima convergence when used to optimize functions with discontinuities. Consequently, we propose to cope with these problems by using the primal dual Newton method that is shown to have better convergence performance as compared to standard Raphson-Newton technique (see details in [31]). We introduce two vectors of extra variables, one for each dimension, and each of them substituting the "most non linear" part of the system in the corresponding direction, namely:

$$w_s^{(c)} = \frac{\partial \psi_s}{\partial u_s} = \frac{u_s}{\psi_s} = \frac{(\mathbf{D}^{(c)}\mathbf{f})_s}{\psi_s} \tag{34}$$

and

$$w_s^{(r)} = \frac{\partial \psi_s}{\partial v_s} = \frac{v_s}{\psi_s} = \frac{(\mathbf{D}^{(r)}\mathbf{f})_s}{\psi_s}. \tag{35}$$

Let us define the vectors of extra variable as:

$\mathbf{w}^{(c)} = [w_1^c, w_2^c, \ldots, w_{m_f n_f}^c]^T$ and $\mathbf{w}^{(r)} = [w_1^r, w_2^r, \ldots, w_{m_f n_f}^r]^T$.

For equation (34), we define a residual term $\boldsymbol{\xi}^{(c)}(\mathbf{f}, \mathbf{w}^{(c)})$ as: $\xi_s^{(c)}(\mathbf{f}, \mathbf{w}^{(c)}) = \psi_s w_s^{(c)} - (\mathbf{D}^{(c)}\mathbf{f})_s$ or equivalently: $\boldsymbol{\xi}^{(c)}(\mathbf{f}, \mathbf{w}^{(c)}) = \boldsymbol{\Psi}(\mathbf{f})\mathbf{w}^{(c)} - \mathbf{D}^{(c)}\mathbf{f}$ where $\boldsymbol{\Psi}(\mathbf{f}) = diag(\psi_s)$. A similar expression is obtained for the $r-$direction. Taking into account equations (32), (34) and (35), one has to solve the linear system

$$\begin{bmatrix} T'(\mathbf{f}, \mathbf{w}^{(c)}, \mathbf{w}^{(r)}) \\ \boldsymbol{\xi}^{(c)}(\mathbf{f}, \mathbf{w}^{(c)}) \\ \boldsymbol{\xi}^{(r)}(\mathbf{f}, \mathbf{w}^{(r)}) \end{bmatrix} = \begin{bmatrix} \mathbf{0} \\ \mathbf{0} \\ \mathbf{0} \end{bmatrix}. \tag{36}$$

This system is globally 'more linear' than the one in equation (31). We compute the Jacobian of this system by means of Taylor series expansion and linearization of the residual terms. So, we can write the linearized system as:

$$\begin{bmatrix} \sum_{k=1}^{K} \mathbf{H}_k^T\mathbf{H}_k & \lambda\mathbf{D}^{(c)^T} & \lambda\mathbf{D}^{(r)^T} \\ \boldsymbol{\Theta}^{(c)} & \boldsymbol{\Psi}(\mathbf{f}) & 0 \\ \boldsymbol{\Theta}^{(r)} & 0 & \boldsymbol{\Psi}(\mathbf{f}) \end{bmatrix} \begin{bmatrix} \delta\mathbf{f} \\ \delta\mathbf{w}^{(c)} \\ \delta\mathbf{w}^{(r)} \end{bmatrix} = - \begin{bmatrix} T'(\mathbf{f}, \mathbf{w}^{(c)}, \mathbf{w}^{(r)}) \\ \boldsymbol{\xi}^{(c)}(\mathbf{f}, \mathbf{w}^{(c)}) \\ \boldsymbol{\xi}^{(r)}(\mathbf{f}, \mathbf{w}^{(r)}) \end{bmatrix} \tag{37}$$

where

$$\boldsymbol{\Theta}^{(c)} = \mathbf{W}^{(c)}\mathbf{W}^{(r)}\mathbf{D}^{(r)} - [\mathbf{I} - \mathbf{W}^{(c)^2}]\mathbf{D}^{(c)},$$

and

$$\boldsymbol{\Theta}^{(r)} = \mathbf{W}^{(r)}\mathbf{W}^{(c)}\mathbf{D}^{(c)} - [\mathbf{I} - \mathbf{W}^{(r)^2}]\mathbf{D}^{(r)}.$$

Now, to solve this system only with respect to $\delta\mathbf{f}$ we apply block elimination to (37) leading to the computation of the Schur complement of matrix $\sum_{k=1}^{K} \mathbf{H}_k^T\mathbf{H}_k$. This transformation is possible as the block $\begin{bmatrix} \boldsymbol{\Psi}(\mathbf{f}) & 0 \\ 0 & \boldsymbol{\Psi}(\mathbf{f}) \end{bmatrix}$ is invertible. We divide the coefficient matrix $\boldsymbol{\Phi}$ of system (37) into four sub-blocks:

$$\boldsymbol{\Phi}_{11} = \sum_{k=1}^{K} \mathbf{H}_k^T\mathbf{H}_k, \ \boldsymbol{\Phi}_{12} = \begin{bmatrix} \lambda\mathbf{D}^{(c)} & \lambda\mathbf{D}^{(r)} \end{bmatrix},$$

$$\boldsymbol{\Phi}_{21} = \begin{bmatrix} \boldsymbol{\Theta}^{(c)} \\ \boldsymbol{\Theta}^{(r)} \end{bmatrix}, \ \boldsymbol{\Phi}_{22} = \begin{bmatrix} \boldsymbol{\Psi}(\mathbf{f}) & 0 \\ 0 & \boldsymbol{\Psi}(\mathbf{f}) \end{bmatrix}.$$

Let $\boldsymbol{\Phi}^S$ denote the Schur complement of $\boldsymbol{\Phi}_{11}$ in $\boldsymbol{\Phi}$:

$$\boldsymbol{\Phi}^S = \boldsymbol{\Phi}_{11} - \boldsymbol{\Phi}_{12}\boldsymbol{\Phi}_{22}^{-1}\boldsymbol{\Phi}_{21}$$

Let $\boldsymbol{\Phi}_{22}^S$ denote the difference between matrices $\boldsymbol{\Phi}^S$ and $\boldsymbol{\Phi}_{11}$:

$$\boldsymbol{\Phi}_{22}^S = -\lambda\mathbf{D}^{(c)^T}\boldsymbol{\Psi}(\mathbf{f})^{-1}\boldsymbol{\Theta}^{(c)} - \lambda\mathbf{D}^{(r)^T}\boldsymbol{\Psi}(\mathbf{f})^{-1}\boldsymbol{\Theta}^{(r)}. \tag{38}$$

We note that if $\boldsymbol{\Phi}_{22}^S$ is symmetric then, the whole matrix $\boldsymbol{\Phi}^S$ is symmetric too. $\boldsymbol{\Phi}_{22}^S$ can be written as:

$$\begin{aligned} \boldsymbol{\Phi}_{22}^S \ &= -\lambda\mathbf{D}^{(c)^T}\boldsymbol{\Psi}(\mathbf{f})^{-1}\boldsymbol{\Theta}^{(c)} - \lambda\mathbf{D}^{(r)^T}\boldsymbol{\Psi}(\mathbf{f})^{-1}\boldsymbol{\Theta}^{(r)} \\ &= -\lambda\mathbf{D}^{(c)^T}\boldsymbol{\Psi}(\mathbf{f})^{-1}[\mathbf{W}^{(c)}\mathbf{W}^{(r)}\mathbf{D}^{(r)} - [\mathbf{I} - \mathbf{W}^{(c)^2}]\mathbf{D}^{(c)}] \ . \\ &\quad -\lambda\mathbf{D}^{(r)^T}\boldsymbol{\Psi}(\mathbf{f})^{-1}[\mathbf{W}^{(r)}\mathbf{W}^{(c)}\mathbf{D}^{(c)} - [\mathbf{I} - \mathbf{W}^{(r)^2}]\mathbf{D}^{(r)}] \end{aligned} \tag{39}$$

This expression shows that $\boldsymbol{\Phi}_{22}^S$ is a symmetric matrix since $\mathbf{W}^{(c)}$, $\mathbf{W}^{(r)}$ and $\boldsymbol{\Psi}(\mathbf{f})$ are diagonal matrices. Consequently, this transformation allows us to solve the system by means of well known iterative methods such as the minimum residual one (Minres) [32], [33]. The Minres function attempts to find a minimum norm residual solution x to the system of linear equations $\mathbf{Ax} = \mathbf{b}$ when matrix $\mathbf{A}$ is symmetric. This condition fits the system that we are studying. In order to solve

the considered system, one can multiply the two bottom row blocks of $\mathbf{\Phi}$ by $\mathbf{\Phi}_{12}\mathbf{\Phi}_{22}^{-1}$ and then subtract from the top block to obtain:

$$(\mathbf{\Phi}_{11} - \mathbf{\Phi}_{12}\mathbf{\Phi}_{22}^{-1}\mathbf{\Phi}_{21})\delta\mathbf{f} = -T'(\mathbf{f}) - \mathbf{\Phi}_{12}\mathbf{\Phi}_{22}^{-1}\begin{bmatrix}\boldsymbol{\xi}^{(c)}\\ \boldsymbol{\xi}^{(r)}\end{bmatrix}.$$

After eliminating the variables $\boldsymbol{\xi}^{(c)}$ and $\boldsymbol{\xi}^{(r)}$ as they represent small residuals, the transformed set of equations to solve to find the descent direction becomes:

$$\mathbf{\Phi}^S\delta\mathbf{f} = -T'(\mathbf{f}). \tag{40}$$

Therefore, the primal-dual Newton method used here consists in finding an appropriate descent direction for the criterion to be minimized. This solution guarantees the decrease of the criterion with respect to all spatial direction when matrix $\mathbf{\Phi}^S = \sum_{k=1}^{K}\mathbf{H}_k^T\mathbf{H}_k + \mathbf{\Phi}_{22}^S$ is positive (semi)-definite. The sum of K matrices $\mathbf{H}_k^T\mathbf{H}_k$ is a positive semi-definite matrix. We have to prove that this is also the case for $\mathbf{\Phi}_{22}^S$. Let $\mathbf{x}$ be a non-zero vector, we introduce $\mathbf{x}^{(c)} = \mathbf{\Psi}(\mathbf{f})^{-1/2}\mathbf{D}^{(c)}\mathbf{x}$ and $\mathbf{x}^{(r)} = \mathbf{\Psi}(\mathbf{f})^{-1/2}\mathbf{D}^{(r)}\mathbf{x}$. According to equation (39), we can write:

$$\begin{aligned}\tfrac{1}{\lambda}\mathbf{x}^T\mathbf{\Phi}_{22}^S\mathbf{x} = {\mathbf{x}^{(c)}}^T[\mathbf{I} - {\mathbf{W}^{(c)}}^2]\mathbf{x}^{(c)} + {\mathbf{x}^{(r)}}^T[\mathbf{I} - {\mathbf{W}^{(r)}}^2]\mathbf{x}^{(r)}\\ -{\mathbf{x}^{(c)}}^T\mathbf{W}^{(c)}\mathbf{W}^{(r)}\mathbf{x}^{(r)} - {\mathbf{x}^{(r)}}^T\mathbf{W}^{(r)}\mathbf{W}^{(c)}\mathbf{x}^{(c)}.\end{aligned} \tag{41}$$

Let denote $\mathbf{y}^{(c)} = \mathbf{W}^{(c)}\mathbf{x}^{(c)}$ and $\mathbf{y}^{(r)} = \mathbf{W}^{(r)}\mathbf{x}^{(r)}$. Equation (41) can be re-written as:

$$\tfrac{1}{\lambda}\mathbf{x}^T\mathbf{\Phi}_{22}^S\mathbf{x} \quad = \quad \left\|\mathbf{x}^{(c)}\right\|_2^2 + \left\|\mathbf{x}^{(r)}\right\|_2^2 - \left\|\mathbf{y}^{(c)} + \mathbf{y}^{(r)}\right\|_2^2. \tag{42}$$

Using Cauchy-Schwartz inequality, and the fact that all elements of diagonal matrices $\mathbf{W}^{(c)}$ and $\mathbf{W}^{(r)}$ are in the interval $[-1,\ 1]$, we can write:

$$\left\|\mathbf{y}^{(c)} + \mathbf{y}^{(r)}\right\|_2^2 \leq \left\|\mathbf{x}^{(c)}\right\|_2^2 + \left\|\mathbf{x}^{(r)}\right\|_2^2. \tag{43}$$

Given the inequality in equation (43) and the equation (42), we conclude that for a given non-zero vector $\mathbf{x}$, $\mathbf{x}^T\mathbf{\Phi}_{22}^S\mathbf{x} \geq 0$. Thus, matrix $\mathbf{\Phi}_{22}^S$ is positive semi-definite and so is $\mathbf{\Phi}^S$. As mentioned earlier, this property guarantees the convergence of the iterative algorithm to the global minimum.

VII. Simulation results

In the following, we test the image restoration performance using regularized MRE and TV-based algorithms. Experiments were carried out for two different images: a portion of Parrot image which has a lot of features and details to be preserved by restoration and the cameraman one which has a homogeneous background with a man in the middle. These images are adequate to measure the ability of the developed algorithms to restore the image details and edges as well as the homogeneous area. In all experiments, the degraded images are altered by a set of PSFs which simulate a camera motion, an averaging action and a gaussian filtering with $\sigma = 1$ and $\sigma = 1.5$, respectively. The number of observed images corresponding to the number of independent PSFs is $K = 4$ and the PSFs' size is 5×5. The degraded images are corrupted by white gaussian additive noise of power σ_n^2. The Signal to Noise Ratio (SNR) is defined as $SNR = 10log_{10}(\frac{\|\mathcal{F}\|_2^2}{\sigma_n^2})$. For the plots on figures 9, 11 and 12, the statistics are evaluated over 100 Monte Carlo runs.

We first propose a comparison between the regularized version of the MRE algorithm and the non regularized one for a set of degraded images with $SNR = 21dB$. The degraded images are shown on figure 3. The image restoration results are depicted on figure 4. This experiment confirms the inefficiency of MRE algorithm in the noisy case. It demonstrates the importance of the regularization to avoid the noise amplification phenomenon associated with the image deconvolution problem.

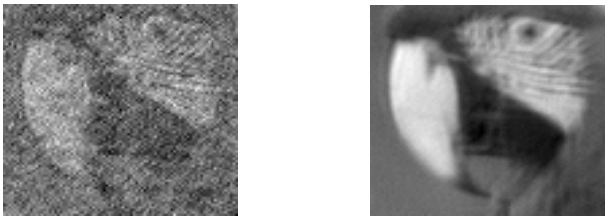

(a) (b)

Fig. 4. (a) MRE restored image (b) R-MRE restored one for observed images on figure 3.

A. R-MRE versus TV-based algorithms

In this experiment, we compare the performance of the two proposed algorithms for the restoration of the Parrot and the Cameraman images, respectively. The R-MRE algorithm with parameters $\mu = 0.5$ for the regularization parameter (equation (16)) and $c = 10\%$ for the relative threshold (equation (15)) has been applied to the degraded images shown on figure 3. The result is compared with the one obtained by the TV-based restoration approach using the channel estimate given by the CR method. The regularization parameters are $\lambda = 6\cdot10^{-3}$ and $\beta = 10^{-4}$. To highlight the performance gain due to the MC processing, we also present in figure 5 the image restored by the monochannel technique in [18] applied to image (a) in figure 3. In this example, we note that the R-MRE algorithm mitigates the noise effect but alters the details of the original image, whereas the TV based method decreases the noise effect while preserving the image texture details . The mono-channel method is almost inefficient since the restored image is similar to the degraded one. The same experiment was conducted on Cameraman image. The set of Cameraman degraded images is shown on figure 6 and the restoration results on figure 7. The parameter values used for the R-MRE algorithm are $\mu = 0.42$ for the regularization parameter and $c = 10\%$ for the relative threshold. Concerning the TV regularization term, the regularization parameter is $\lambda = 5\cdot10^{-3}$ and the disturbing scalar is $\beta = 10^{-4}$. We also display in figure 8 a log-compressed version of the degraded and restored images in order to highlight the restored image details. Note that details like the cameraman hand is missing in the degraded image whereas it is visible in the TV-based restored image.

The last part of this experiment is a comparative study of the performance of R-MRE and TV-based algorithms versus the

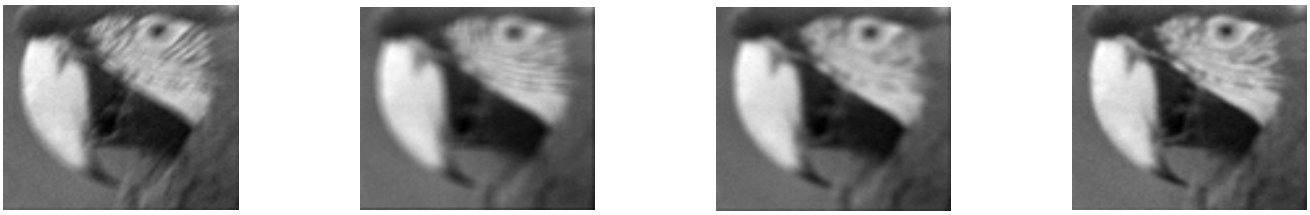

(a) (b) (c) (d)

Fig. 3. Blurred noisy observed images with PSFs (a) motion filter (b) average filter (c) gaussian filter with variance 1 (d) gaussian filter with variance 1.5 and SNR=21dB.

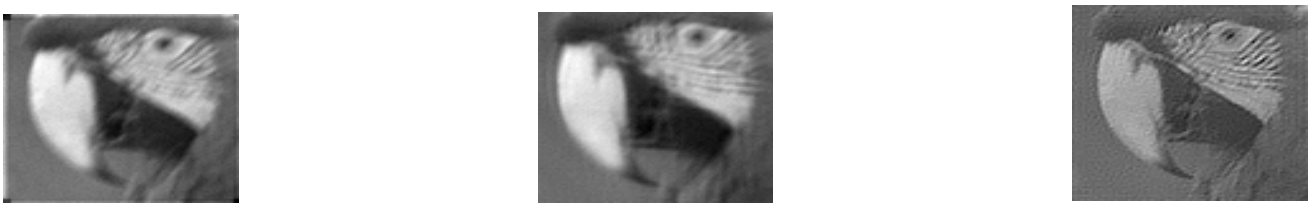

(a) (b) (c)

Fig. 5. Restored images using different algorithms (a) a regularized monochannel method (b) R-MRE algorithm (c) TV-based algorithm

(a) (b) (c) (d)

Fig. 6. Blurred noisy observed images with PSFs (a) motion filter (b) average filter (c) gaussian filter with variance 1 (d) gaussian filter with variance 1.5 and SNR=22dB.

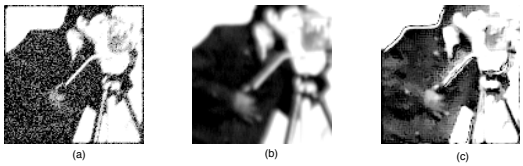

Fig. 8. Log-compressed images for visual purposes corresponding to (a) one degraded image (b) R-MRE restored image (c) TV-based restored image.

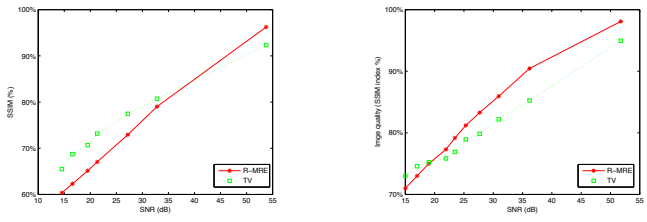

(a) (b)

Fig. 9. Objective quality of the restored image by means of R−MRE and TV regularization, respectively, versus SNR for (a) Parrot image, (b) Cameraman image.

SNR values in the range $[15\ 55]dB$. To avoid manual choice of the regularization parameters, we have chosen them according to the following rule: $c = 10\%$, $\beta = 10^{-4}$, $\mu = \frac{10^4}{SNR^4}$ and $\lambda = \frac{55}{SNR^3}$. Indeed, this 'ad hoc' choice is to reduce the weight of the regularization term when the SNR level increases. Figure 9 shows the evolution of the restored image quality with respect to the SNR. The objective quality of the restored image is evaluated by means of a structural objective image quality index namely the Structural Similarity Index Measure (SSIM) introduced in [34]. For this experiment, some remarks are done and several conclusions could be drawn.

Remark 1: This experiment has been carried on two different kinds of images. Parrot image has many details (Parrot face details). On the opposite, cameraman image has a homogeneous background with a cameraman in the middle. It is expected that the performance of both algorithms is different for each kind of image. In order to see this difference, we fixed the whole parameters the same way for both images. Namely, parameters λ and μ depend only on the SNR.

Remark 2: Concerning R-MRE algorithm, when the images are

(a) (b) (c)

Fig. 7. Restored images using different algorithms (a) restored image using a regularized monochannel method applied to image (a) of figure 6 (b) R-MRE restored image (c) TV-based restored image.

too noisy (low SNR) if the same 'big amount' of regularization is applied to restore Parrot and cameraman images, it seems then predictable that the Parrot image have worse quality than cameraman. In fact, in this case the regularization (large value of μ) also 'destroys' the details in Parrot image. This remark explains the fact that for low SNRs, Parrot image similarity index is in the interval $[60\%\ 70\%]$ whereas cameraman image similarity index is in the interval $[70\%\ 80\%]$.

Remark 3: The performance of R-MRE and TV-based restoration algorithms highly depends on the image nature, the amount of noise and the parameters selection. In future work, we will thoroughly evaluate the sensitivity of the latter with respect to the choice of different parameters. But, in this stage of the work, we could propose to use the algorithms depending on the image nature and the SNR as depicted on figure 10.

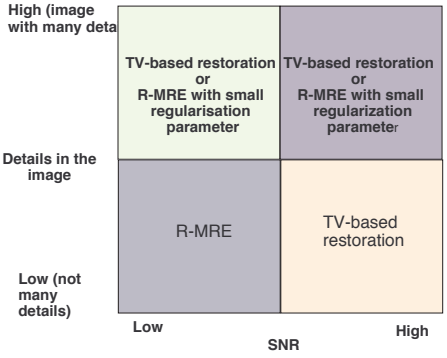

Fig. 10. The choice of restoration method with respect to SNR value and image type.

B. Identification performance

Our objective here is the performance study of the blind identification of the channel parameter vector $\mathbf{h}$ given the blurred images $\mathbf{g}_1, \ldots, \mathbf{g}_K$. Indeed, channel estimation errors may result in significant degradation of the restored image quality. Hence, we disturb the channel vector $\mathbf{h}$ by adding $\epsilon\Delta\mathbf{h}$ where ϵ is a varying positive scalar and $\Delta\mathbf{h}$ a fixed random vector of unit norm. Hence, $\hat{\mathbf{h}} = \mathbf{h} + \epsilon\Delta\mathbf{h}$ represents the blur function used for image restoration by means of TV-based method in VI. The restored image quality is measured using the SSIM. Figure 11 illustrates the degradation of the restored image quality due to channel identification disturbance. As we can observe, this degradation becomes significant when the channel estimation error ($\| \epsilon\Delta\mathbf{h} \|^2$) is larger than ($-10dB$). In our work, we have used several methods to identify the PSF

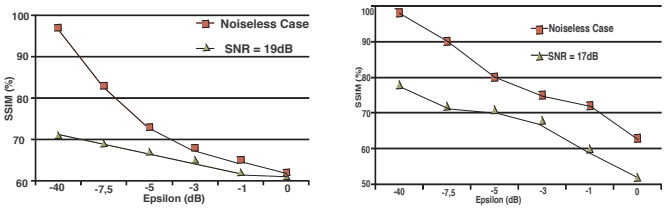

(a) (b)

Fig. 11. Impact of the channel identification precision on the restored image quality for (a) Parrot image, (b) Cameraman image.

coefficients. A comparison between these methods is given on figure 12. We compare the channel estimation performance of the considered methods for different SNR values. More precisely, we plot the mean value of Normalized Mean Square Error (NMSE) between the estimated and the actual PSF vector parameter: $10log_{10}(\frac{\|\mathbf{h}_{est}-\mathbf{h}\|^2}{\|\mathbf{h}\|^2})$ as a function of the SNR for the SS, MNS, SMNS, CR and LSS methods. To do so, we fix the original image, but we generate randomly the K filters at each Monte Carlo run. Surprisingly, the CR method (which is the less expensive one) outperforms the other methods. This is due probably to the fact that all other methods use the eigen-subspaces of large ill-conditioned matrices and hence are very sensitive to noise effect.

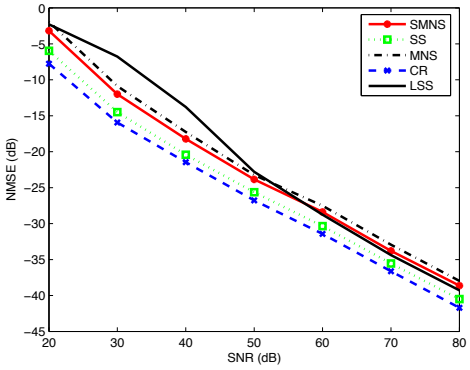

Fig. 12. Channel estimation MSE versus SNR: $-0-$ SMNS,... SS, _..._ MNS,$-*-$ CR,$-$ LSS.

C. Comparison to the state of the art

In this section we carry out a comparative study between the methods proposed in this article and the iterative MBD method in [10]. The first experiment is performed with the cameraman degraded images on figure 6. The result is depicted on figure 13.

This figure shows that while the R-MRE methods removes more noise it smooths image edges. TV based method and the iterative one proposed in [10] have similar results. When we compare the cameraman jacket on figures 13-(b) and 13-(c) we can see that the TV-based method removes more noise from the degraded images.

VIII. Conclusions and future work

In this article, we focus on efficient techniques aiming at restoring an original image using several degraded renditions of it. This paper introduces two multichannel restoration techniques with regularization. The first one is a direct restoration technique based on regularized MRE algorithm. The MRE algorithm ensures a perfect restoration of the original image in the noiseless case, but is inefficient in presence of noise. Hence, in the noisy case, the MRE algorithm was used jointly with an appropriate regularization technique that improves significantly its performance even at low and moderate SNRs. The second restoration technique consists in the identification of the degradation filters before their inversion. Several deterministic identification algorithms were tested including a version of the LSS method that is generalized here from the 1D to the 2D case. The estimated PSFs are then exploited to restore the original image using a least squares criterion jointly with a Total Variation term that mitigates the noise amplification effect. Efficient optimization with convergence study of the TV-based criterion was considered. Simulation comparisons of the two proposed restoration techniques are provided for different SNR ranges and for different image types using an objective image quality metric. In a future work, several issues will be deepened. We will study the sensitivity of the proposed methods towards the selection of parameters. We will also use real-life images to further evaluate the performance of the proposed methods.

References

[1] Gregory A. Showman and James H. McClellan, "Blind polarimetric equalization of ultrawideband synthetic aperture radar imagery," in *ICIP*, 2000.

[2] A. Jalobeanu, L. Blanc-Féraud, and J. Zerubia, "Hyperparameter estimation for satellite image restoration using a mcmc maximum likelihood method," *Pattern Recognition*, vol. 35, pp. 341–352, 2002.

[3] Yulia V. Zhulina, "Multiframe blind deconvolution of heavily blurred astronomical images," *Applied Optics*, vol. 45, no. 28, pp. 7342–7352, Oct. 2006.

[4] Šroubek Filip, Šimberová Stanislava, Flusser Jan, and Suk Tomáš, "Multichannel blind deconvolution of the short-exposure astronomical images," in *Proceedings of the International Conference on Pattern Recognition*, Sep. 2000, vol. 3, pp. 53–56.

[5] M. Vrhel and B.L. Trus, "Multi-channel restoration of electron micrographs," in *Proceedings of the International Conference on Image Processing*, Oct. 1995, vol. 2, pp. 516–519.

[6] H. J. Trussel, M. I. Sezan, and D. Tran, "Sensitivity of color lmmse restoration of images to the spectral estimation," *IEEE Trans. on Signal Processing*, vol. 39, no. 1, pp. 248–252, Jan. 1991.

[7] U.A. Al Suwailem and J. Keller, "Multichannel image identification and restoration using continuous spatial domain modeling," in *Proc. ICIP*, Oct. 1997.

[8] F. Sroubek and J. Flusser, "Multichannel blind deconvolution of spatially misaligned images," *IEEE Trans. on Image Processing*, vol. 14, no. 7, pp. 874– 883, July 2005.

[9] N. P. Galatsanos, A. K. Katsaggelos, R. T. Chin, and A. D. Hillery, "Least squares restoration of multichannel images," *IEEE Trans. Acoust., Speech, Signal Processing*, vol. 39, pp. 2222–2236, Oct. 1991.

[10] F. Sroubek and J. Flusser, "Multichannel blind iterative image restoration," *IEEE Trans. on Image Processing*, vol. 12, no. 9, pp. 1094– 1106, Sep. 2003.

[11] C.A. Ong and J.A. Chambers, "An enhanced NAS-RIF algorithm for blind image deconvolution," *IEEE Trans. on Image Processing*, vol. 8, no. 7, pp. 988–992, July 1999.

[12] W. Souidene, K. Abed-Meraim, and A. Beghdadi, "Deterministic techniques for multichannel blind image deconvolution," in *Proc. ISSPA*, Aug. 2005.

[13] L. Tong and Q. Zhao, "Joint order detection and blind channel estimation by least squares smoothing," *IEEE Trans. on Signal Processing*, vol. 47, pp. 2345–2355, Sept 1999.

[14] E. Fishler, A. Haimovich, R. Blum, D. Chizhik, L. Cimini, and R. Valenzuela, "MIMO radar: An idea whose time has come," in *Proc. IEEE Radar Conference*, Apr. 2004.

[15] B. Hassibi, B. M. Hochwald, and T. L. Marzetta, "Multi-antenna wireless communications - from theory to algorithms," in *Proc. IEEE ICASSP*, May 2002.

[16] D. G. Karakos and P. E. Trahanias, "Generalized multichannel image-filtering structures," *IEEE Trans. on Image Processing*, vol. 6, pp. 1038–1045, July 1997.

[17] G. B. Giannakis and R. W. Heath, "Blind identification of multichannel fir blurs and perfect image restoration," *IEEE Trans. on Image Processing*, vol. 9, no. 11, Nov. 2000.

[18] D.S.C. Biggs and M. Andrews, "Acceleration of iterative image restoration algorithms," *Applied Optics*, vol. 36, no. 8, 1997.

[19] A. Beghdadi and B. Pesquet-Popescu, "A new image distortion measure based on wavelet decomposition," in *Proc. ISSPA*, July 2003.

[20] W. Souidene, K. Abed-Meraim, and A. Beghdadi, "Blind multichannel image deconvolution using regularized MRE algorithm: performance evaluation," in *Proc. ISSPIT*, Dec. 2004.

[21] Wirawan, "Multichannel image blind restoration: second order methods," *PhD Thesis report*, 2002.

[22] M.K. Ng, R.J. Plemmons, and S. Qiao, "Regularization of rif blind image deconvolution," *IEEE Trans. on Image Processing*, vol. 9, pp. 1130–1134, June 2000.

[23] A. Mayer, A. Castiaux, and J. P. Vigneron, "Electronic green scattering with n-fold symmetry axis from block circulant matrices," *Computer Physics Communications*, vol. 109, pp. 81–89, Mar. 1998.

[24] G. J. Tee, "Eigenvectors of block circulant and alternating circulant matrices," *New Zealand Journal of Mathematics*, vol. 8, pp. 123–142, 2005.

[25] Wirawan, K. Abed-Meraim, H. Maitre, and P. Duhamel, "Blind multichannel image restoration using subspace based method," in *Proc. ICASSP*, 2003.

[26] Y. Hua, K. Abed-Meraim, and M. Wax, "Blind system identification using minimum noise subspace," *IEEE Trans. on Signal Processing*, vol. 45, no. 3, March 1997.

[27] G. Harikumar and Y. Bresler, "Exact image deconvolution from multiple fir blurs," *IEEE Trans. Image Processing*, vol. 8, no. 6, pp. 846–862, 1999.

[28] G. Harikumar and Y. Bresler, "Perfect blind restoration of images blurred by multiple filters: Theory and efficient algorithms," *IEEE Trans. Image Process.*, vol. 8, pp. 202–219, Feb. 1999.

[29] Rudin L. I., Osher S. J., and Fatemi, "Nonlinear total variation based noise removal algorithms," *Physica D*, vol. 60, pp. 259–268, 1992.

[30] A. K. Jain, *Fundamentals of digital image processing*, 1989.

[31] Tony F. Chan, Gene H. Golub, and Pep Mulet, "A nonlinear primal-dual method for total variation-based image restoration," in *ICAOS '96*, Berlin, Germany / Heidelberg, Germany / London, UK / etc., 1996, vol. 219, pp. 241–252, Springer-Verlag.

[32] C. Paige and M. Saunders, "Solution of sparse indefinite systems of linear equations," *SIAM J. Numer. Anal.*, vol. 12, pp. 259–268, 1975.

[33] B. Fisher, *Polynomial Based Iteration Methods for Symmetric Linear Systems*, 1996.

[34] Z. Wang, E.P. Simoncelli, and A.C. Bovik, "Multi-scale structural similarity for image quality assessment," in *Proc. IEEE Asilomar Conference*, Nov. 2003.

(a) (b) (c)

Fig. 13. Objective quality of the restored image by means of (a) R−MRE, (b) TV regularization, (c) iterative MBD method in [10] with 10 iterations.